Materials Advances

ROYAL SOCIETY OF CHEMISTRY

COMMUNICATION

View Article Online
View Journal | View Issue

Cite this: *Mater. Adv.*, 2021, 2, 2918

Received 9th February 2021,
Accepted 5th April 2021

DOI: 10.1039/d1ma00120e

rsc.li/materials-advances

Carbon coated cobalt oxide (CC-Co_3O_4) as electrode material for supercapacitor applications

Rahul Kumar, *[a] Ankur Soam[b] and Veena Sahajwalla[a]

Carbon coated cobalt oxide (CC-Co_3O_4) was prepared by colloidal processing using cobalt oxide and sucrose. Sucrose was used as a soluble carbon precursor in the preparation of CC-Co_3O_4. CC-Co_3O_4 was characterized by Brunauer–Emmett–Teller (BET) analysis, X-ray diffraction (XRD), Raman spectroscopy, Scanning electron microscopy (SEM), Transmission electron microscopy (TEM), and X-ray photoelectron spectroscopy (XPS) respectively. Electrochemical properties of CC-Co_3O_4 were measured in 1 M KOH electrolyte. CC-Co_3O_4 exhibited the maximum specific capacitance of 395 F g^{-1} at a scan rate of 5 mV s^{-1}. The enhanced electrochemical performance of CC-Co_3O_4 may be due to the increased conductivity of the composite electrode by carbon coating over the cobalt oxide nanoparticles.

1. Introduction

The market for hybrid electric vehicles and portable electronic devices is growing very fast and consequently there is a need for high-power energy storage system to be integrated to the devices.[1] An energy device which has high energy density and can be discharged quickly upon demand is good for energy storage. To fulfil the growing energy demands of society for human activities, several efforts have been given to fabricate high performance and energy-producing storage devices. In energy storage devices, supercapacitors (SCs) are promising for energy storage due to their high-power density (PD), easy fabrication, and long cycling life.[2–4]

SCs can be categorized into three different types according to the charge storage phenomenon: the electric double layer capacitor (EDLC), the pseudocapacitor, and the hybrid supercapacitor. In EDLC, the charges are stored at the electrode and electrolyte interfaces, electrostatically *via* reversible adsorption of ions from the electrolyte at the electrode surface, whereas in the pseudocapacitor, charges are stored faradaically by electron transfer between electrode and electrolyte resulting in higher specific capacitance than that of EDLC.

Pseudocapacitors utilize transition metal oxides or conducting polymers as electrode materials. Transition metal oxide materials are one of the most promising electrodes for energy storage devices due to high theoretical specific capacitance, high specific surface area, electrical conductivity, electro-active sites, chemical stability, ample reserves, and environmental friendliness.[5–10] There are many different oxides such as RuO_2, IrO_2, MnO_2, Co_2O_3, NiO, V_2O_5, SnO_2, TiO_2, and Fe_2O_3 *etc.*, which are used for fabrication of electrodes for supercapacitors.[11–20]

Cobalt oxide (Co_3O_4) has attracted a lot of attention for its use in various applications such as energy storage devices, catalysis, and electrochemical sensors because of its unique properties such as high reversibility and theoretical specific capacitance (3560 F g^{-1}) and controllable morphology compared with the bulk phase.[21–23] Co_3O_4 is a potential candidate due to its unique properties and may be an alternate to expensive RuO_2 which is broadly used as the electrochemically active material in electrochemical capacitors.[24]

The metal oxide/carbon composites have been fabricated including carbon nanotubes, carbon nanofibers, graphene, and amorphous carbon materials, which dramatically improved the electroconductivity and further enhanced the specific capacitance and rate performances of the metal oxide/carbon composites.[25–30]

In this work, cobalt oxide slurry was prepared using cobalt oxide and sucrose, sucrose was used as a soluble carbon source in the slurry. Sucrose has converted into conducting carbon during annealing and coated on cobalt oxide particles. Electrochemical properties of CC-Co_3O_4 were investigated for supercapacitor application.

2. Experimental

2.1. Synthesis of CC-Co_3O_4

Sucrose (Molecular formula (C_{12},$H_{22}O_{11}$), Merck-Germany) and Cobalt oxide (Molecular Formula (Co_3O_4) Sigma Aldrich) were

[a] *Centre for Sustainable Materials Research and Technology, School of Materials Science and Engineering, University of New South Wales, NSW 2052, Australia. E-mail: kumarrahul003@gmail.com*
[b] *Department of Mechanical Engineering, Siksha 'O' Anusandhan University, Khandagiri Square, Bhubaneswar-751030, Odisha, India*

used to fabricate the CC-CO_3O_4. First PVA (1 wt%) (Sigma Aldrich, Mol. weight = 100 000) solution was prepared in water and then sucrose was added in the solution. PVA was used as a binder for fabrication of the CC-CO_3O_4. Cobalt oxide was added to the sucrose containing solutions separately. The mixture was kept on the magnetic stirrers for 24 h for stirring. The homogeneous suspension of cobalt oxide was obtained, and suspension was dried at 150 °C in oven for 24 h to remove the water. After drying and crushing of mixtures, sucrose coated powder of the cobalt oxide was obtained. Sucrose would be yielded 8 wt% of carbon in CC-CO_3O_4 after annealing of the samples.[31–34] Annealing of the sucrose coated powder was done in flowing argon at 650 °C. The annealed powder was used to investigate the electrochemical properties of CC-CO_3O_4.

2.2. Characterization

The properties of CC-CO_3O_4 were examined by using the various equipment such as multi-point Brunauer–Emmett–Teller (BET) analysis, X-ray diffraction (XRD)(Model-PANalytical X'Pert Pro multipurpose XRD), Raman spectroscopy (Model-Renishaw Invia Raman Microscope), Scanning electron microscope (SEM) (Model-TM 3000 Hitachi), Transmission electron microscopy (TEM) (Model-JEOL JEM-2100F), and X-ray photoelectron spectroscopy (XPS) (Model-Thermo ESCALAB250i).

The electrochemical properties of the CC-CO_3O_4 electrodes were studied using cyclic voltammetry (CV), galvanostatic charge–discharge (GCD) measurements and electrochemical impedance spectroscopy (EIS) on Autolab Potentiostat/Galvanostatic (Biologic VSP-300) electrochemical work-station with a three electrode cell.

3. Results and discussion

3.1. Surface, XRD, Raman, morphology, and chemical compositional analysis of CC-CO_3O_4

Nitrogen adsorption/desorption experiments were carried out on the CC-CO_3O_4.[29,30] BET method was used to determine the total surface area. For the mesopore surface area, pore volume and pore diameter, the Barrett–Joyner–Halenda (BJH) method was used. The corresponding isotherms and pore size distributions are demonstrated in Fig. 1(a and b). All the nitrogen adsorption/desorption isotherms are 'type I' isotherms as shown by the steep rise in adsorbed volume of N_2. The trait of I-type curves (Fig. 1a) in CC-CO_3O_4 is confirmed by steep uptake of nitrogen ($P/P_0 < 0.05$), manifesting copious micropores.[35,36] The average pore diameters Dads and Ddes (Dads and Ddes are the average pore diameters for BJH adsorption and desorption) were found to be 4.94 and 4.77 nm respectively. Surface area of the CC-CO_3O_4 was found to be 16.88 $m^2\ g^{-1}$.

XRD was used to analyse the crystalline components of CC-CO_3O_4 operating at 40 kV and 40 mA and measurements were recorded from an angle (2θ = 10° to 90°), with total accumulation time of around 60 min. Fig. 1(c) shows a XRD pattern of CC-CO_3O_4, a diffraction peak can be seen at about 26.2° and this peak is assigned to the (0 0 2) planes of

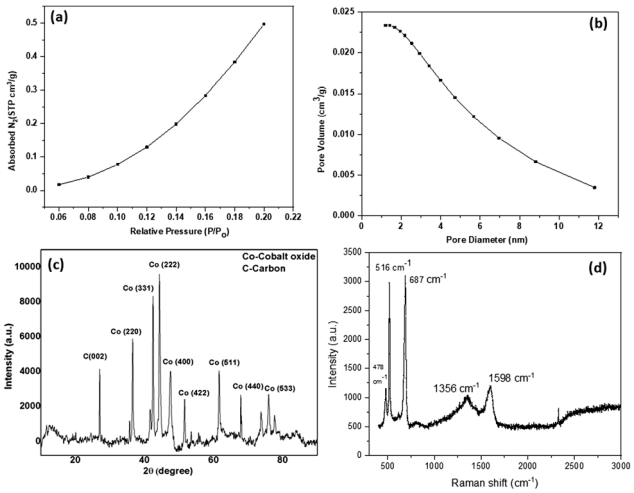

Fig. 1 (a) Nitrogen adsorption/desorption isotherms, (b) Nitrogen desorption/desorption pore size distribution (c) XRD patterns, and (d) Raman spectra of CC-CO_3O_4.

hexagonal graphite structure. The diffraction peaks at 31.3°, 36.8°, 44.8°, 55.65°, 59.4°, 65.2°, and 77.34° can be perfectly indexed to cobalt oxide (111), (220), (311), (400), (422), (511), (440), and (533) planes of cubic structure (PDF card: 42-1467), respectively. XRD data confirms the formation of CC-CO_3O_4.[37,38]

Raman spectroscopy was carried out to extend the study for the carbon structures in CC-CO_3O_4 which are shown in Fig. 1(d), where the peaks of Raman spectrum of Co_3O_4 anchored on the carbon derived from sucrose at 516, 478 and 687 cm^{-1}, can be attributed to the E_g, F_{2g} and A_{1g} modes of cobalt oxide.[37,38] It is noted that there are two remarkable peaks around 1356 and 1598 cm^{-1} refer to the D-band (arising from the edge or defect sites of carbon) and G band (representing the sp^2 carbon) of the graphitic domain, respectively.[39–43]

SEM and TEM were used to characterize the morphology of the CC-CO_3O_4 as shown in Fig. 2. SEM images (a & b) show that the particles are nonuniform in size and most of the particles are in the range of 10–80 μm. The smaller particles in Fig. 2(a and b) are the carbon particles and bigger particles are carbon coated cobalt oxide particles. TEM images of carbon-coated cobalt oxide particles are presented in Fig. 2(c and d). These images further reveal the presence of carbon-coated cobalt particles in the sample. The particles are composed of a metal oxide core and a carbon shell. The cobalt oxide particles are encapsulated in a 2–3 nm thick carbon layer as demonstrated in Fig. 2(e) (inserted figure). The carbon shell presented in the particles has graphitic structure as shown in Fig. 2(e). The diffraction pattern (Fig. 2(f)) shows the crystalline nature of CC-CO_3O_4.

XPS (Model-Thermo ESCALAB250i) was carried out on CC-CO_3O_4. In the XPS analysis, The Al Kα line was used as the X-ray source. For measurements, samples were loaded into ultra-high vacuum (about 2×10^{-9} mbar) chamber of the XPS apparatus.

X-ray photoelectron spectroscopy (XPS) was further performed to analyze the chemical environment of various elements in carbon coated cobalt oxide. From the XPS survey spectrum of

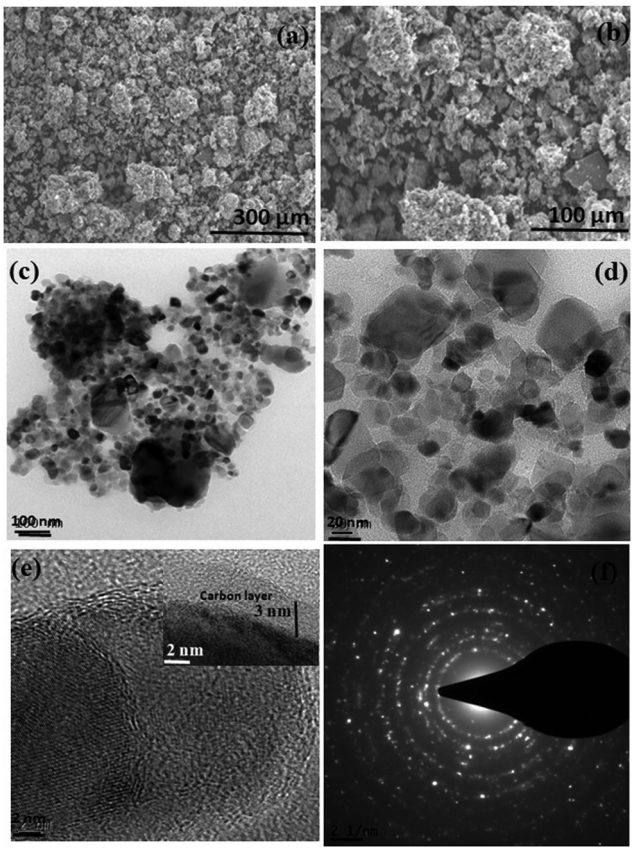

Fig. 2 SEM images (a) and (b) at high magnification, TEM images at low and high magnifications, (c) TEM image at low magnification, (d) and (e) TEM image at high magnification, and (f) SAED patterns of CC-Co_3O_4.

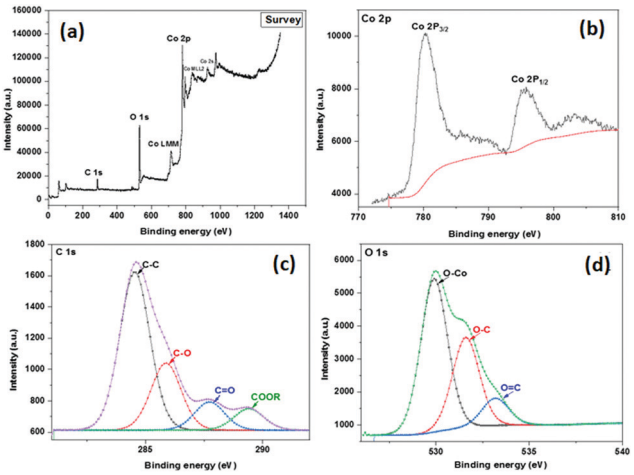

Fig. 3 XPS of CC- Co_3O_4 (a) Survey scan, (b) Co 2p spectrum, (c) C 1s spectrum, and (d) O 1s spectrum.

carbon coated cobalt oxide, the Co, C and O elements are detected as shown in Fig. 3(a). The XPS spectrum for Co 2p shown in Fig. 3(b) reveals two major peaks with binding energies at 780.3 and 795.8 eV, corresponding to Co $2p_{3/2}$ and Co $2p_{1/2}$, respectively, with a spin energy separation of 15.3 eV, which is attributed to the Co^{2+} oxidation state, indicating that a portion of Co^{3+} is reduced to Co^{2+} with generating oxygen vacancies.[44] These results again confirmed that Co_3O_4 nanoparticles have been anchored on carbon derived from sucrose, Co^{2+} and Co^{3+} in the crystal structure of Co_3O_4 are being considered to be playing a vital role in improving catalytic performance of oxygen reduction reaction and oxygen evolution reaction.[45]

As shown in Fig. 3(c), the C1s peak can be resolved into three different component peaks, representing C–C (284.7 eV), C–O (285.8 eV), C═O (287.7 eV), and COOR (289.5 eV) groups, respectively.[46] The O1s spectrum (Fig. 3(d)) can be divided into three main types of chemical states. The peaks at 529.9 eV, 531.5 eV and 533.3 eV are ascribed to O–Co, O–C and O═C bonding, respectively.[47]

3.2. Electrochemical analysis of CC-CO_3O_4

Further, the electrochemical performance of CC-CO_3O_4 as electrodes was studied with cyclic voltammetry (CV), galvanostatic charging/discharging process and electrochemical impedance spectroscopy (EIS). Biologic VSP 300 electrochemical workstation, with a three-electrode cell was employed to do these measurements. A saturated calomel electrode (SCE) was used as the reference electrode and platinum wire works as the counter electrode in a three-electrode cell. The sample for the electrochemical measurements was prepared by mixing 1 mg of each CC-CO_3O_4 with 10 μL of Nafion perfluorinated resin solution separately, respectively.[20] The samples paste was made and then pasted on the platinum electrode which was then used as a working electrode. Electrolyte, 1 M aqueous KOH solution was prepared using KOH salt and DI water. CV experiments were carried out at the scan rates ranging between 5 and 50 mV s^{-1} in the potential window of 0.0 to +0.6 V. The following eqn (1) was used to calculate the specific gravimetric capacitance (C, F g^{-1}) of CC-CO_3O_4 from the CV curves.

$$C = \frac{\text{Area under the CV curve (mA V}^{-1})}{2 \times \text{scan rate (mV s}^{-1}) \times \text{potential window } (V) \times \text{mass of CC-Co}_3\text{O}_4\text{ (g)}} \quad (1)$$

The cyclic voltammetry (CV) curves of CC-CO_3O_4 are demonstrated in Fig. 4(a) and the specific capacitance values calculated from the CV curves using eqn (1) are shown in Fig. 4(b). It can be observed from Fig. 4(a) that as the scan rate increases, current increases, CC-CO_3O_4 exhibits higher current densities with a higher san rate. These are the characteristics of a capacitor. CC-CO_3O_4 electrode exhibited a specific capacitance of 395 F g^{-1} at scan rate of 5 mV s^{-1}. The capacitance values were observed to decrease significantly with increasing the scan rate for CC-CO_3O_4 as demonstrated in Fig. 4(b). The capacitance value for CC-CO_3O_4 dropped from 395 to 75 F g^{-1} when the scan rate was increased from 5 to 50 mV s^{-1}. Co^{2+} and Co^{3+} in the crystal structure of Co_3O_4 are being considered to be playing a vital role in improving catalytic performance of

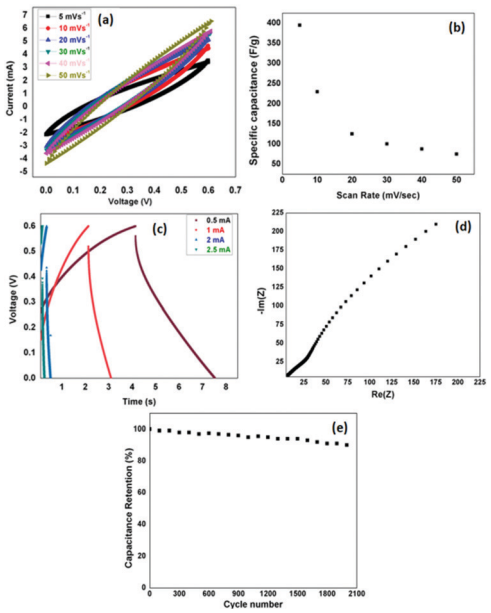

Fig. 4 (a) CV curves recorded at the scan rate of 5, 10, 20, 30, 40, and 50 mV s^{-1}, (b) Specific capacitance as a function of scan rate, (c) Charging and discharging curves measured at current densities of 0.5, 1, 2 and 2.5 mA, (d) Nyquist plot, and (e) cycle stability of CC-Co_3O_4 respectively.

oxygen reduction reaction and oxygen evolution reaction.[45] Actually, the continuous conversion between Co^{2+} and Co^{3+} in the crystal structure of Co_3O_4 is beneficial to the redox reaction for charge storage. At lower scan rates, the electrolyte ions have adequate time to infiltrate into the pores of CC-CO_3O_4, whereas at higher scan rates, the ions store only on the outer surface due to slow ion diffusion.[48] For that reason, higher scan rates result in lower capacitance value. The rate capability of the CC-Co_3O_4 electrode may be enhanced by choosing the right concentration of carbon in the electrode. Actually, the rate capability of an electrode depends on many factors like conductivity and porosity of the electrode *etc.* From the SEM and TEM images (Fig. 2), it is observed that the carbon present at the surface of the Co_3O_4 nanoparticles. However, the non uniform coating of carbon on Co_3O_4 may also be responsible for the poor rate capability of the CC-Co_3O_4 electrode.

The GCD curves of CC-CO_3O_4 electrode at different current values are shown in Fig. 4(c). The voltage and time curves for CC-CO_3O_4 are almost linear, which indicates that the electrode exhibited capacitive behaviour. The charge/discharge duration decreases with the current values from 0.5 to 2.50 mA. GCD curves of CC-CO_3O_4 appear nearly triangular in shape; this result informs a typical, electrical double-layer capacitive behaviour. CC-Co_3O_4 exhibits good capacitance as observed in CV measurements.

The charge-storage mechanism of the CC-Co_3O_4 electrode in KOH solution is as follows.[49]

$$Co_3O_4 + OH^- + H_2O \leftrightarrow 3CoOOH + e^- \quad (2)$$

$$CoOOH + OH^- \leftrightarrow CoO_2 + H_2O + e^- \quad (3)$$

The electrochemical performance of CC-Co_3O_4 was further studied by using electrochemical impedance spectroscopy (EIS).

Table 1 Comparison of the specific capacitances of cobalt oxide materials reported in literature

Electrode	Capacitance (F g^{-1})	Scan rate (mV s^{-1})	Ref.
Co_3O_4 Nanocubes	430.0	10	52
Co_3O_4/SWNT	313.9	1	53
Co_3O_4-PPy-rGO	532.8	5	54
Co_3O_4 nanosphere	128	10	55
Co_3O_4 thin film	74	5	56
Co_3O_4 nanoparticles	304.0	5	57
CC-Co_3O_4	395.0	5	Present work

EIS Nyquist plot of CC-Co_3O_4 is demonstrated in Fig. 4(d). The experiment was performed at the frequency range from 0.1 Hz to 5 MHz. The Nyquist plot includes an almost inclined straight line started from high to low frequency. A vertical line proves ideal super capacitive behavior, which is a symbol of the diffusion of ions at the interface between the electrolyte and the electroactive materials.[50,51] A line that is more perpendicular toward the imaginary *y*-axis demonstrates that the supercapacitor behaves similarly to an ideal capacitor.[50] The almost vertical line of CC-Co_3O_4 leans more toward the *y*-axis which reveals that CC-Co_3O_4 has excellent electrochemical behavior. The series resistance was calculated and it was found to be 4 Ohm for CC-Co_3O_4 electrode. The comparison of the capacitance of CC-CO_3O_4 electrode with the reported literature is given in Table 1.[52–57]

The cycle stability test for the sample was performed by repeating charging/discharging cycles. The capacitance retention with cycle numbers is shown in Fig. 4(e). We have determined the capacitance retention up to 2000 cycles. It can be seen that the electrode exhibited good capacitance retention while charging/discharging the device many times.[39] It showed 90% retention in capacitance up to 2000 cycles. The above results suggested that the electrode may be used for high-performance supercapacitors.

4. Conclusions

In conclusion, CC-Co_3O_4 has been fabricated using sucrose as a soluble source of carbon and cobalt oxide by colloidal processing. The *in situ* formation of carbon coated on cobalt oxide particles may enhance the electrical conductivity, which improves the electrochemical performance of the electrode. The carbon coating and well connected cobalt oxide network would help to provide continuous electron transfer pathways, improving the conductivity of the electrode. However, rate capability of the CC-Co_3O_4 electrode can further be improved by finding the right concentration of the carbon in the composite. The maximum specific capacitance of CC-Co_3O_4 was found 395 F g^{-1} at 5 mV s^{-1}. These results suggested that CC-Co_3O_4 may play a significant role as an electrode material for energy storage application.

Conflicts of interest

There are no conflicts to declare.

Acknowledgements

This work was supported by SMaRT Centre. The authors acknowledge the access to experimental facilities at Mark Wainwright Analytical Centre, University of New South Wales, Australia.

References

1 P. G. Bruce, S. A. Freunberger, L. J. Hardwick and J. M. Tarascon, Li–O_2 and Li–S Batteries with High Energy Storage, *Nat. Mater.*, 2012, **11**, 19–29.
2 P. G. Bruce, B. Scrosati and J. M. Tarascon, Nanomaterials for Rechargeable Lithium Batteries, *Angew. Chem., Int. Ed.*, 2008, **47**, 2930–2946.
3 B. L. Ellis and L. F. Nazar, Sodium and Sodium-Ion Energy Storage Batteries, *Curr. Opin. Solid State Mater. Sci.*, 2012, **16**, 168–177.
4 G. Z. Chen, Supercapacitor and supercapattery as emerging electrochemical energy stores, *Int. Mater. Rev.*, 2017, **62**, 173–202.
5 G. Wang, L. Zhang and J. Zhang, A review of electrode materials for electro-chemical supercapacitors, *Chem. Soc. Rev.*, 2012, **2**, 41797–41828.
6 G. Yu, L. Hu, N. Liu, H. Wang, M. Vosguerichian, Y. Yang, Y. Cui and Z. Bao, Enhancing the Supercapacitor Performance of Graphene/MnO2 Nanostructured Electrodes by Conductive Wrapping, *Nano Lett.*, 2011, **11**, 4438–4442.
7 Q. Lu, J. Chen and J. Xiao, Nanostructured Electrodes for High-Performance Pseudocapacitors, *Angew. Chem., Int. Ed.*, 2013, **52**, 1882–1889.
8 T. Brousse, D. Belangeer and J. W. Long, To Be or Not To Be Pseudocapacitive?, *J. Electrochem. Soc.*, 2015, **162**, A5185–A5189.
9 Y. Jiang and J. Liu, Definitions of Pseudocapacitive Materials: A Brief Review, *Energy Environ. Mater.*, 2019, **2**, 30–37.
10 Y. Gogotsi, Energy Storage in Nanomaterials – Capacitive, Pseudocapacitive, or Battery-like?, *ACS Nano*, 2018, **12**, 2081–2083.
11 Y. R. Ahn, M. Y. Song, S. M. Jo, C. R. Park and D. Y. Kim, Electrochemical capacitors based on electrodeposited ruthenium oxide on nanofibre substrates, *Nanotechnology*, 2006, **12**, 2865–2869.
12 C. C. Hu, Y. H. Huang and K. H. Chang, Annealing effects on the physicochemical characteristics of hydrous ruthenium and ruthenium-iridium oxides for electrochemical supercapacitors, *J. Power Sources*, 2002, **108**, 117–127.
13 R. Kumar, B. K. Singh, A. Soam, S. Parida and P. Bhargava, *In situ* carbon coated manganese oxide nanorods (ISCC-MnO2NRs) as an electrode material for supercapacitors, Dia. Rel, *Materials*, 2019, **94**, 110–117.
14 S. G. Kandalkar, J. L. Gunjakar and C. D. Lokhande, Preparation of cobalt oxide thin films and its use in supercapacitor application, *Appl. Surf. Sci.*, 2008, **254**, 5540–5544.
15 U. M. Patil, R. R. Salunkhe, K. V. Gurav and C. D. Lokhande, Chemically deposited nanocrystalline NiO thin films for supercapacitor application, *Appl. Surf. Sci.*, 2008, **255**, 2603–2607.
16 R. Kumar, A. Soam and V. Sahajwalla, Sucrose-derived carbon-coated nickel oxide (SDCC-NiO) as an electrode material for supercapacitor applications, *Mater. Adv.*, 2020, **1**, 609–616.
17 C. C. Hu, Y. H. Huang and K. H. Chang, Anodic deposition of porous vanadium oxide net- work with high power characteristics for pseudocapacitors, *J. Power Sources*, 2008, **1851**, 594–1597.
18 R. Kumar and R. K. Nekouei, Veena Sahajwalla, *In situ* carbon-coated tin oxide (ISCC-SnO2) for micro-supercapacitor applications, *Carbon Lett.*, 2020, **30**, 699–707.
19 R. Kumar, B. K. Singh, A. Soam, S. Parida, V. Sahajwalla and P. Bhargava, *In situ* carbon supported titanium dioxide (ICS-TiO2) as electrode material for high performance supercapacitors, *Nanoscale Adv.*, 2020, **2**, 2376–2386.
20 R. Kumar, A. Soam, R. Hussian, I. Mansuri and V. Sahajwalla, Carbon coated iron oxide (CC-IO) as high performance electrode material for supercapacitor applications, *J. Energy Storage*, 2020, **32**, 101737.
21 C. Yuan, L. Yang, L. Shen, X. Zhang and W. Lou, Growth of ultrathin mesoporous Co3O4 nanosheet arrays on Ni foam for high-performance electrochemical capacitors, *Energy Environ. Sci.*, 2012, **5**, 7883.
22 H. Cheng, Z. G. Lu, J. Q. Deng, C. Y. Chung, K. Zhang and Y. Y. Li, A facile method to improve the high rate capability of Co_3O_4 nanowire array electrodes, *Nano Res.*, 2010, **3**, 895.
23 T. Y. Wei, C. H. Chen, K. H. Chang, S. Y. Lu and C. C. Hu, Cobalt oxide aerogels of ideal supercapacitive properties prepared with an epoxide synthetic route, *Chem. Mater.*, 2009, **21**, 3228.
24 C. C. Hu, K. H. Chang, M. C. Lin and Y. T. Wu, Design and Tailoring of the Nanotubular Arrayed Architecture of Hydrous RuO_2 for Next Generation Supercapacitors, *Nano Lett.*, 2006, **6**, 2690.
25 B. Babakhani and D. G. Ivey, Anodic deposition of manganese oxide electrodes with rod-like structures for application as electrochemical capacitors, *J. Power Sources*, 2010, **195**, 2110–2117.
26 X. T. Guo, Y. Z. Zhang, F. Zhang, Q. Li, D. H. Anjum, H. F. Liang, Y. Liu, C. Liu, H. N. Alshareef and H. Pang, A novel strategy for the synthesis of highly stable ternary SiOx composites for Li-ion-battery anodes, *J. Mater. Chem. A*, 2019, **7**, 15969.
27 X. R. Li, J. L. Wei, Q. Li, S. S. Zhang, Y. X. Xu, P. Du, C. Y. Chen, J. Y. Zhao, H. G. Xue, Q. Xu and H. Pang, Nitrogen-Doped Cobalt Oxide Nanostructures Derived from Cobalt–Alanine Complexes for High-Performance Oxygen Evolution Reactions, *Adv. Funct. Mater.*, 2019, **28**, 1800886.
28 L. Miao, Z. Song, D. Zhu, L. Li, L. Gun and M. Liu, Recent advances in carbon-based supercapacitors, *J. Mater. Adv.*, 2020, **1**, 945–966.
29 J. Yan, L. Miao, H. Duan, D. Zhu, Y. Lv, W. Xiong, L. Li, L. Gan and M. Liu, Core-shell hierarchical porous carbon spheres with N/O doping for efficient energy storage, *Electrochim. Acta*, 2020, **358**, 136899.
30 L. Miao, H. Duan, D. Zhu, Y. Lv, L. Gan, L. Li and M. Liu, Boron ''gluing'' nitrogen heteroatoms in a prepolymerized ionic liquid-based carbon scaffold for durable supercapacitive activity, *J. Mater. Chem. A*, 2021, **9**, 2714–2724.

31 R. Kumar and P. Bhargava, Synthesis and characterization of low specific resistance alumina-clay–carbon composites by colloidal processing using sucrose as a soluble carbon source for electrical applications, *RSC Adv.*, 2016, **6**, 8705–8713.
32 R. Kumar and P. Bhargava, Fabrication of low specific resistance ceramic carbon composites by colloidal processing using glucose as soluble carbon source, *Bull. Mater. Sci.*, 2017, **40**, 1197–1202.
33 R. Kumar and Parag Bhargava, Fabrication of low specific resistance ceramic carbon composites by slip casting Asi, *Cer. Societies*, 2015, **3**, 262–265.
34 R. Kumar, M. Singh and A. Soam, Study on electrochemical properties of Silicon micro particles as electrode for supercapacitor application, *Surf. Interfaces*, 2020, **19**, 100524.
35 L. Miao, D. Zhu, Y. Zhao, M. Liu, H. Duan, W. Xiong, Q. Zhu, L. Li, Y. Lv and L. Gan, Design of carbon materials with ultramicro-, supermicro- and mesopores using solvent- and self-template strategy for supercapacitors, *Microporous Mesoporous Mater.*, 2017, **253**, 1–9.
36 Z. Zhou, L. Miao, H. Duan, Z. Wang, Y. Lv, W. Xiong, D. Zhu, L. Li, M. Liu and L. Gan, Highly active N, O-doped hierarchical porous carbons for high-energy supercapacitors, *Chin. Chem. Lett.*, 2020, **31**, 1226–1230.
37 Z. Zhang, L. Li, Q. Xu and B. Cao, 3D hierarchical Co3O4 microspheres with enhanced lithium-ion battery performance, *RSC Adv.*, 2015, **5**, 61631–61638.
38 M. Wang, *et al.*, Co_3O_4 nanorods decorated reduced graphene oxide composite for oxygen reduction reaction in alkaline electrolyte, *Electrochem. Commun.*, 2013, **34**, 299–303.
39 A. Soam, R. Kumar, P. K. Sahoo, M. C. B. Kumar, N. Arya, M. Singh, S. Parida and R. O. Dusane, Synthesis of Nickel Ferrite Nanoparticles Supported on Graphene Nanosheets as Composite Electrodes for High Performance Supercapacitor, *ChemistrySelect*, 2019, **4**, 9952–9958.
40 R. Kumar and P. Bhargava, Fabrication of a counter electrode using glucose as carbon material for dye sensitized solar cells, *Mater. Sci. Semicond. Process.*, 2015, **40**, 331–336.
41 R. Kumar and P. Bhargava, Synthesis and characterization of carbon based counter electrode for dye sensitized solar cells (DSSCs) using organic precursor 2-2′ Bipyridine (Bpy) as a carbon material, *J. Alloys Compd.*, 2018, **748**, 905–910.
42 R. Kumar, V. Sahajwalla and P. Bhargava, Fabrication of a counter electrode for dye-sensitized solar cells (DSSCs) using carbon material produced by organic ligand 2-Methyl-8-hydroxyquinolinol (Mq), *Nanoscale Adv.*, 2019, **1**, 3292–3299.
43 R. Kumar, A. Raj, S. Mitra and P. Bhargava, Carbon derived from sucrose as anode material for lithium-ion batteries, *J. Electron. Mater.*, 2019, **48**, 7389–7395.
44 L. Xu, *et al.*, Plasma-Engraved Co3O4 Nanosheets with Oxygen Vacancies and High Surface Area for the Oxygen Evolution Reaction, *Angew. Chem., Int. Ed.*, 2016, **55**, 5277–5281.
45 Y. X. Zhang, X. Guo, X. Zhai, Y. M. Yan and K. N. Sun, Diethylenetriamine (DETA)-assisted anchoring of Co_3O_4 nanorods on carbon nanotubes as efficient electrocatalysts for the oxygen evolution reaction, *J. Mater. Chem. A*, 2015, **3**, 1761–1768.
46 X. Tang, Q. Feng, J. Huang, K. Liu, X. Luo and Q. Peng, *J. Colloid Interface Sci.*, 2018, **510**, 368–375.
47 S. Y. Zhao, C. X. Li, J. Liu, N. Y. Liu, S. Qiao and Y. Z. Han, Carbon quantum dots/SnO_2–Co_3O_4 composite for highly efficient electrochemical water oxidation, *Carbon*, 2015, **92**, 64–73.
48 T. Liu, F. Zhang, Y. Song and Y. Li, Revitalizing carbon supercapacitor electrodes with hierarchical porous structures, *J. Mater. Chem.*, 2017, **5**, 17705–17733.
49 L. Tao, L. Shengjun, Z. Bowen, W. Bei, N. Dayong, C. Zeng, Y. Ying, W. Ning and Z. Weifeng, Supercapacitor electrode with a homogeneously Co_3O_4-coated multiwalled carbon nanotube for a high capacitance, *Nanoscale Res. Lett.*, 2015, **10**, 208.
50 Y. Wang, Z. Shi, Y. Huang, Y. Ma, C. Wang, M. Chen and Y. Chen, Supercapacitor devices based on graphene materials, *J. Phys. Chem. C*, 2009, **13**, 13103–13107.
51 J. W. Lee, J. M. Ko and J. D. Kim, Hydrothermal preparation of nitrogen-doped graphene sheets *via* hexamethylenetetramine for application as supercapacitor electrodes, *Electrochim. Acta*, 2012, **85**, 459–464.
52 G. S. Jang, S. Ameen, M. S. Akhtar and H. S. Shin, Cobalt oxide nanocubes as electrode material for the performance evaluation of electrochemical supercapacitor, *Ceram. Int.*, 2018, **44**, 588–595.
53 M. B. Durukan, R. Yuksel and H. E. Unalan, Cobalt Oxide Nanoflakes on Single Walled Carbon Nanotube Thin Films for Supercapacitor Electrodes, *Electrochim. Acta*, 2016, **222**, 1475–1482.
54 L. L. Jiang, Y. J. Li, D. Luo, Q. Y. Zhang, F. G. Cai, G. J. Wan, L. Xiong and Z. F. Ren, Freestanding RGO–Co_3O_4–PPy Composite Films as Electrodes for Supercapacitors, *Energy Technol.*, 2019, **7**, 1800606.
55 Y. Duan, T. Hu, L. Yang, J. Gao, S. Guo, M. Hou and X. Ye, Facile fabrication of electroactive microporous Co_3O_4 through microwave plasma etching for supercapacitors, *J. Alloys Compd.*, 2019, **771**, 156–161.
56 V. R. Shinde, S. B. Mahadik, T. P. Gujar and C. D. Lokhande, Supercapacitive cobalt oxide (Co_3O_4) thin films by spray pyrolysis, *Appl. Surf. Sci.*, 2006, **252**, 7487–7492.
57 Z. Y. Li, P. T. M. Bui, D. H. Kwak, M. S. Akhtar and O. B. Yang, Enhanced electrochemical activity of low temperature solution process synthesized Co_3O_4 nanoparticles for pseudo-supercapacitors applications, *Ceram. Int.*, 2016, **42**, 1879–1885.